Received: 11 October 2023 | Revised: 27 February 2024 | Accepted: 26 April 2024

High Voltage

DOI: 10.1049/hve2.12488

ORIGINAL RESEARCH

Research on temperature distribution characteristics of oil-immersed power transformers based on fluid network decoupling

Yongming Xu[1] | Ziyi Xu[1] | Congrui Ren[2] | Yaodong Wang[3]

[1]School of Electrical and Information Engineering, Changzhou Institute of Technology, Changzhou, China

[2]School of Electrical and Electronic Engineering, Harbin University of Science and Technology, Harbin, China

[3]Department of Engineering, Durham University, Durham, UK

Correspondence

Yongming Xu, School of Electrical and Information Engineering, Changzhou Institute of Technology, Changzhou 213032, China.
Email: xuyongming@czu.cn

Associate Editor: Weigen Chen

Funding information

National Natural Science Foundation of China, Grant/Award Number: 52077047; Natural Science Foundation of the Jiangsu Higher Education Institutions of China, Grant/Award Number: 22KJA470002

Abstract

Due to the complex structure and large size of large-capacity oil-immersed power transformers, it is difficult to predict the winding temperature distribution directly by numerical analysis. A 180 MVA, 220 kV oil-immersed self-cooling power transformer is used as the research object. The authors decouple the internal fluid domain of the power transformer into four regions: high voltage windings, medium voltage windings, low voltage windings, and radiators through fluid networks and establish the 3D fluid-temperature field numerical analysis model of the four regions, respectively. The results of the fluid network model are used as the inlet boundary conditions for the 3D fluid-temperature numerical analysis model. In turn, the fluid resistance of the fluid network model is corrected according to the results of the 3D fluid-temperature field numerical analysis model. The prediction of the temperature distribution of windings is realised by the coupling calculation between the fluid network model and the 3D fluid-temperature field numerical analysis model. Based on this, the effect of the loading method of the heat source is also investigated using the proposed method. The hotspot temperatures of the high-voltage, medium-voltage, and low-voltage windings are 89.43, 86.33, and 80.96°C, respectively. Finally, an experimental platform is built to verify the results. The maximum relative error between calculated and measured values is 4.42%, which meets the engineering accuracy requirement.

1 | INTRODUCTION

Power transformer is one of the most important components in the power system, and its safe and stable operation for a long time is crucial [1, 2]. However, transformer life is directly related to the winding temperature, and most transformer failures are caused by high winding temperatures [3, 4]. Therefore, fast and accurate prediction of transformer winding temperature is of great significance to prolong the transformer life and ensure the stable operation of the power system, which has received a lot of attention from scholars.

The existing predominant approaches for predicting power transformer temperatures include the numerical analysis method, the empirical formula method, and the lumped parameter method.

Radakovic et al. [5, 6] constructed fluid and thermal network models based on the structural characteristics of different cooling methods of transformers, respectively. The thermal resistance and temperature of the thermal network nodes were assessed using the solution of the fluid network. Finally, the thermal network model (THNM) was solved to obtain the transformer winding temperature rise. In the subsequent research, the researchers employed the aforementioned methodology to compute the temperature distribution of the transformer across various load circumstances and ascertain the transformer's resistance to overloading [7].

Researchers expanded the fluid-THNM to incorporate the variable pressure chamber. The accuracy of THNM is further improved by considering the air thermal buoyancy and airflow pressure loss in the construction of the fluid network model of the variable pressure chamber and by constructing a THNM that includes the walls and the roof [8]. Cotas et al. [9] investigated the effect of dynamic changes in fluid velocity on fluid network parameters by numerical analysis. It was found that the flow resistance can respond quickly when the fluid velocity changes, and a dynamic fluid network model was developed. Zhou et al. [10] developed a transient THNM for a dry-type on-board traction transformer that can account for wind speed and load fluctuation, and verified the accuracy of the model through experiment. Taheri et al. [11] used non-linear parameters to consider the effects of transformer oil density, thermal conductivity, specific heat capacity, and dynamic viscosity on the calculation accuracy of the THNM and improved the hotspot temperature calculation model for transformer windings. Shiravand et al. [12, 13] added the radiator temperature node between its ambient temperature node and top oil temperature node to solve the problem that the empirical calculation model of the transformer winding hotspot temperature did not consider the radiator and gave the relevant equation for temperature rise calculation. Taheri et al. [14] established a THNM containing the radiation heat source based on the Fourier definition and gave the calculation formula for calculating the hotspot temperature. Although a lot of improvements have been made to improve the calculation accuracy, the influence of the thermophysical properties of the fluid with temperature on the calculation results has not been considered enough.

Wei et al. [15] used the finite volume method to analyse the transformer temperature field and simplified the split-cooled transformer model by increasing the surface heat dissipation coefficient. The effect of the distance between the radiator and the oil tank on the hotspot temperature rise of the winding was also investigated. Silva et al. [16] simplified the transformer model by merging the insulation and wires of the winding, neglecting the thickness of the tank, the pulling plate, and the clamps, and obtained the internal temperature distribution of the transformer by solving the Fourier-Kirchhoff equation numerically. The authors in refs. [17, 18] combined the solid structures in the winding into a single unit to simplify the transformer numerical analysis model and achieve the full-domain temperature rise prediction. Córdoba et al. [19] constructed a full-domain three-dimensional model of the transformer and used a uniform porous medium instead of windings to obtain the fluid flow rate and temperature distribution inside the transformer. Stebel et al. [20] established the 1/2 electromagnetic model of the transformer and the fluid-thermal models of the 1/16 winding and 1/4 tank and realised the transformer temperature field prediction by transferring the oil flow rate and temperature in the two fluid-thermal models. The effects of cooling medium type and ambient temperature on transformer temperature distribution and oil flow characteristics were also investigated. Liu et al. [21] first established a three-dimensional fluid field numerical analysis model near the lower yoke of the transformer core to calculate the winding inlet flow rate, used the results as boundary conditions to calculate the two-dimensional temperature field of the winding model, and obtained the two-dimensional temperature distribution of the winding. Chi et al. [22] developed a three-dimensional flow-thermal analysis model for transformer windings. The mathematical model for solving the temperature and pressure of the oil tank and radiator is constructed based on the analytical method. By transferring the thermal state of the oil flow between the 3D model and the mathematical model, the transformer winding temperature distribution is obtained. Raeisian et al. [23] modelled the fluid and solid regions of the transformer separately. The fluid domain model was solved using the heat flux as the boundary condition, and the results were used as convective boundary conditions to solve the solid domain model. The results of the solid domain calculations were used to correct the fluid boundary heat fluxes, and iterative calculations were performed to obtain the transformer temperature distribution. Finally, the fin size is adjusted based on the response surface method to suppress the winding hot spot temperature. Dasara et al. [24] verified the suppression effect of a new magnetic shunt on the hot spot temperature of the power transformer by 3D finite element analysis. The aforementioned research utilising the numerical analysis approach has achieved significant advancements in the estimation of the temperature field in windings. However, the utilisation of a full-domain numerical model poses challenges in accurately accounting for the winding details. Moreover, the method of decoupling the partition of the transformer and then coupling the calculation by adjacent boundary conditions has more iterations and takes longer to calculate.

In light of those mentioned above, an oil-immersed power transformer is used as a research object in this paper. The fluid domain of the transformer is decoupled based on the fluid network. A 3D fluid-temperature field numerical model is developed for the high, medium, and low voltage windings and the radiator, respectively. The fluid network is solved, and the results are used as the boundary conditions of the numerical analysis model. The fluid network flow resistance parameters are corrected by the results of the numerical analysis model to consider the fluid thermophysical property change. In this way, the respective advantages of the lumped parameter method and the numerical analysis method can be fully combined and utilised. Finally, the winding temperature distribution of the oil-immersed power transformer is obtained by the bi-directional coupling between the fluid network and the 3D fluid-temperature field model.

2 | METHODOLOGY

2.1 | Prototype parameters

The research object of this paper is a three-phase, five-column oil-immersed self-cooling power transformer. The main parameters are shown in Table 1.

TABLE 1 Power transformer main parameters.

Items		Value
Capacity (MVA)		180
Voltage level (kV)		220
High-voltage windings	Turns number	570
	Segments number	102
	Winding type	Inner screen continuous/ continuous
	Axial dimension (mm)	13.88
	Inner (mm)/outer diameter (mm)	1473/1702
	Radial dimension (mm)	114.5
Medium-voltage windings	Turns number	305
	Segments number	78
	Winding type	Continuous
	Axial dimension (mm)	18.97
	Inner (mm)/outer diameter (mm)	1118/1336
	Radial dimension (mm)	109
Low-voltage windings	Turns number	48
	Segments number	96
	Winding type	Double helix
	Axial dimension (mm)	15.18
	Inner (mm)/outer diameter (mm)	956/1014
	Radial dimension (mm)	29
Radiators	Type	PC 2700-30/520
	Quantity (group)	32
	Number of pieces	30
	Height (mm)/width (mm)	2700/520
Core	Height (mm)	2140
	Width (mm)	920

When the oil-immersed self-cooling power transformer runs, the windings and core generate a lot of losses, which are all converted into heat. The transformer oil absorbs the heat generated in the windings and core, and the temperature rises, resulting in a lower density. The difference in buoyancy caused by the difference in density makes the hot transformer oil rise to the top of the tank and enter the radiator through the upper inlet of the radiator. Through the radiator, the transformer oil releases the absorbed heat to the outside and then back to the transformer through the lower outlet of the radiator, which realises the self-cooling. The transformer structure and internal oil flow path are shown in Figure 1, and ϑ_{yc}, ϑ_{rc}, ϑ_{rr} in the diagram are used to mark the positions.

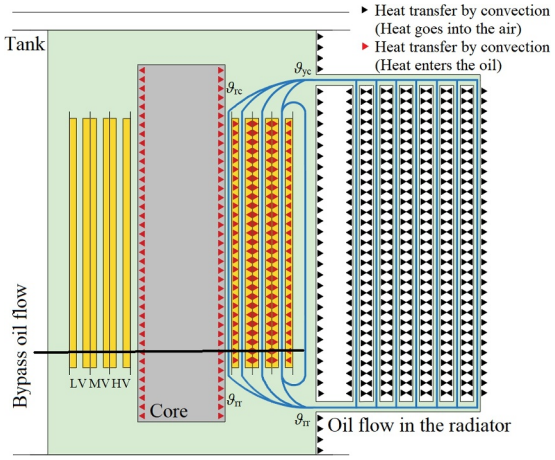

FIGURE 1 Transformer structure and internal oil flow path.

2.2 | Fluid network model

In constructing the fluid network model for oil-immersed self-cooling transformers, the following assumptions are made:

1. The loss is evenly distributed along the axial direction, and the mainstream flow direction of the oil is axial. Thus, in solving the fluid network, the oil temperature in the winding is linearly distributed in the axial direction.
2. The thermal conductivity of the paper cylinder among the high voltage winding, medium voltage winding, and low voltage winding is extremely small. This results in very little heat transfer among high voltage winding, medium voltage winding, and low voltage winding. Almost all of the copper loss is absorbed by the transformer oil. Therefore, the paper cylinder is considered to be adiabatic [25].
3. Since the pipe between the oil tank and the radiator is short and there are no heat sinks on the outer surface of the pipe, the temperature change of the transformer oil in the pipe between the oil tank and the radiator is ignored.

According to the law of energy conservation, when the transformer reaches a steady state, the relationship between the gravitational pressure drop of the oil flow and the resistance pressure drop is shown below:

$$\Delta P_r = \Delta P_g = \oint_l \rho \vec{g} d\vec{h} \tag{1}$$

where ΔP_r is the total resistance pressure drop of the oil flow path, ΔP_g is the gravity pressure drop of the oil flow path, l is the closed path curve of the oil flow path, ρ is the oil density, $\vec{g}$ is the gravitational acceleration, and $\vec{h}$ is the component of l along the direction of gravity.

The flow resistance in the transformer fluid network model can be divided into three types: oil flow resistance in the winding, oil flow resistance in tank, and oil flow resistance in the radiator. Compared with the oil flow resistances in the

winding and in the radiator, the oil flow resistance in the tank is relatively small, so the effect of temperature change on the resistance pressure drop is ignored when calculating the oil flow resistance in the tank. The resistance pressure drop in the tank is calculated using Equation (2) [26].

$$\Delta P = \frac{4fL}{D} \times \frac{U^2}{2}\rho \tag{2}$$

where ΔP is the resistance pressure drop, f is the average dimensionless friction coefficient of fluid duct, L is the fluid duct length, D is the equivalent hydraulic diameter of fluid duct, ρ is the fluid density, and U is the average flow velocity of fluid duct.

The flow resistance of radiator and windings is solved by numerical analysis. The density of the transformer oil in Equation (1) can be calculated using Equation (3).

$$W = \rho_{av} c_p Q_O \Delta T \tag{3}$$

where W is the loss value within the structure, ρ_{av} is the density of the oil flow at the average temperature of the oil flow, c_p is the specific heat capacity of transformer oil, Q_O is the flow rate of transformer oil, and ΔT is the temperature difference.

The inflow and outflow of each node in the fluid network model are equal as shown in Equation (4):

$$\sum_{i=1}^{n} Q_i = 0 \tag{4}$$

The fluid network model is established according to the transformer oil flow path as shown in Figure 2. ΔP is the pressure loss of oil flow. P_g is the gravity of oil flow. Subscript LV is the low-voltage winding. Subscript MV is the medium-voltage winding. Subscript HV is the high-voltage winding. Subscript C is the iron core. Subscript OBP is the bypass oil flow. Subscript CC is the radiator. Subscript cb-wb is the oil flow inlet from the bottom of the iron core to the bottom of the winding. Subscript wt-ct is the outlet from the top of the winding to the top of the iron core. Subscript cb-ti is the inlet from the bottom of the iron core to the oil tank. Subscript ct-to is the inlet from the oil tank to the top of the iron core. Subscript CB is the bottom of the iron core. Subscript PCO and PHO are top pipe and bottom pipe between oil tank and the radiator, respectively.

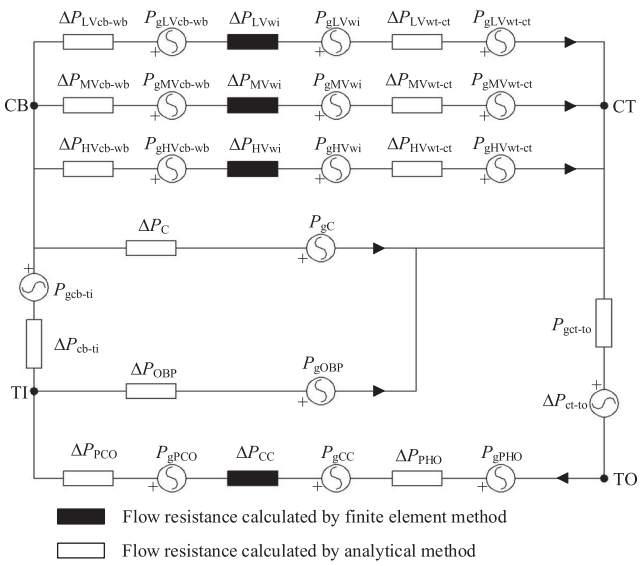

FIGURE 2 Fluid network model of the transformer.

By solving the fluid network, the flow rate of each oil flow branch and the temperature distribution of the transformer oil at each location can be obtained. The results of the fluid network will be used as boundary conditions for the 3D fluid-temperature field numerical analysis.

2.3 | Fluid-temperature field numerical analysis model

To realise the transformer winding temperature prediction, the transformer is decoupled into four regions: high-voltage winding, medium-voltage winding, low-voltage winding, and radiator by the fluid network according to the structural characteristics and oil flow path of the transformer. A 3D fluid-temperature field numerical analysis model is established and solved for each region separately, and the software used for the numerical analysis is Ansys Fluent 2020 R2. The temperature characteristics of the transformer winding can be obtained, and the fluid resistance in the fluid network model can be corrected according to the numerical analysis results.

To improve the calculation speed of numerical analysis, the following simplifications and assumptions are made about the physical model.

1. The three-phase winding of a transformer is a three-phase symmetrical circuit. The frequencies and amplitudes of the voltages and currents of the different phase windings are equal, and only the phases are different. Therefore, this paper takes one-phase winding as an example for analysis.
2. It is assumed that the symmetric position in the transformer has the same fluid state and temperature distribution [27].
3. The single-phase winding is symmetrical in the circumferential direction along the plane formed by the centreline of the pad and the brace.
4. The winding between two planes formed by the centreline of adjacent pads and spacers is the smallest unit of rotational symmetry.
5. Natural convective heat transfer boundary conditions are imposed on the external surface of the transformer tank to simulate the heat transfer process between the external surface of the tank and the ambient environment. The ambient temperature is measured through experiment.
6. The Reynolds number of the transformer oil inside the winding and radiator is less than 2000. Therefore, the oil flow is in laminar flow.

The 3D physical models of the minimum symmetric unit of the high-voltage winding, medium-voltage winding, and low-voltage winding are established, respectively as shown in Figure 3a. Among them, the high-voltage winding structure is the most complex, and the top section of the high-voltage winding is shown in Figure 3b. Since the symmetric position is assumed to have the same fluid state and temperature distribution, only one radiator is modelled. The radiator physical model is shown in Figure 3c.

To discretise the mesh, ANSYS Fluent Meshing 2020R2 is utilised. The utilisation of polyhedral mesh technology allows for efficient control over the overall number of meshes, while simultaneously ensuring a relatively good mesh quality. This, in turn, facilitates the enhancement of solution speed. Therefore, polyhedral mesh is used to fine delineate each three-dimensional physical model of the transformer as shown in Figure 4. Furthermore, greater emphasis is placed on areas exhibiting substantial variations or small-scale geometric characteristics. The use of a conformal mesh is implemented to enhance the precision of numerical analysis. The meshes exhibit a maximum skewness of 6.8×10^{-1}, a minimum skewness of 1.2×10^{-3}, and an average skewness of 5.3×10^{-2}. These values suggest that the meshes constructed have a low degree of skewness, which is a feature of high-quality meshes. Furthermore, a mesh independence verification is performed to guarantee that the results are not influenced by the generated mesh. The total number of meshes ranged from 5 million to 20 million in order to compare the hotspot and average temperature of the high-voltage, medium-voltage, and low-voltage windings. Ultimately, the reference model consists of 9.6 million meshes, with a discrepancy of less than 1% between the hotspot and average temperature.

After the 3D modelling and mesh generation of the windings and radiator, the fluid-temperature field of the four regions is solved according to the calculation results of the fluid network. In turn, the fluid network is corrected according to the fluid-temperature field result. Finally, the simulation is conducted on a Dell workstation T7920 with 2 × Intel Xeon Gold 6248R and 512 GB DDR4 memory.

2.4 | Coupled solution of fluid network model and numerical analysis model

Except for the transformer oil inlet and outlet, all other positions of the winding are covered by insulating paper cylinders and insulating end rings. For the radiator, it only performs transformer oil exchange with the transformer through the inlet at the top and the outlet at the bottom. Therefore, the windings and radiator are decoupled from the transformer full-domain fluid-thermal analysis by using the inlet and outlet of the windings and radiator in the fluid network model as decoupling points. The velocity and temperature of the transformer oil at the decoupling points are used as boundary conditions for the numerical analysis to solve for the fluid field-temperature field distribution of the four regions. Subsequently, the flow resistance in the fluid network model is corrected according to the numerical analysis results. The variation of physical properties of the transformer oil with temperature is shown in Figure 5. The calculation is iterated

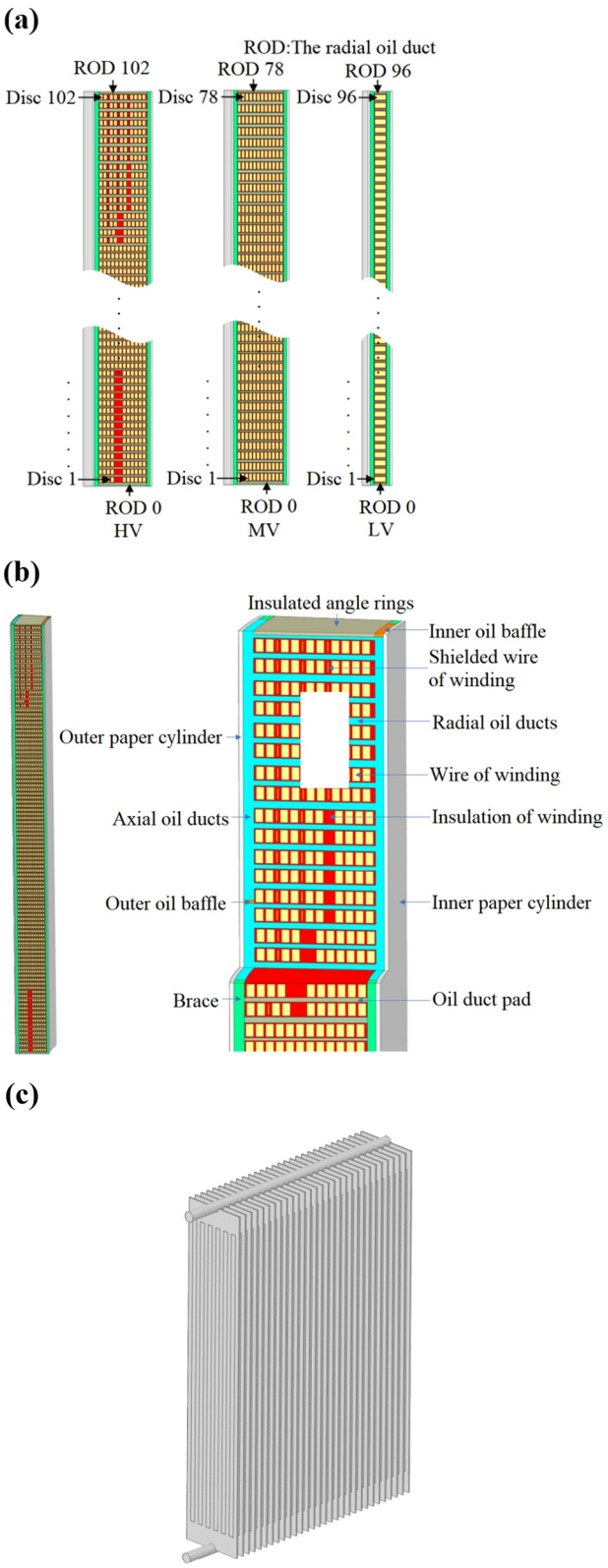

FIGURE 3 3D physical model. (a) High-voltage, medium-voltage and low-voltage windings. (b) Top section of high-voltage winding. (c) Radiator.

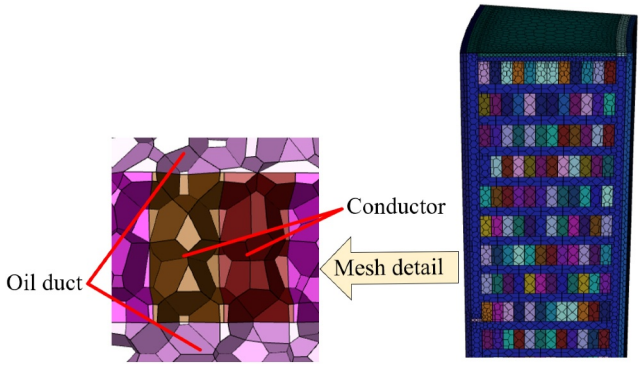

FIGURE 4 Schematic diagram of mesh division.

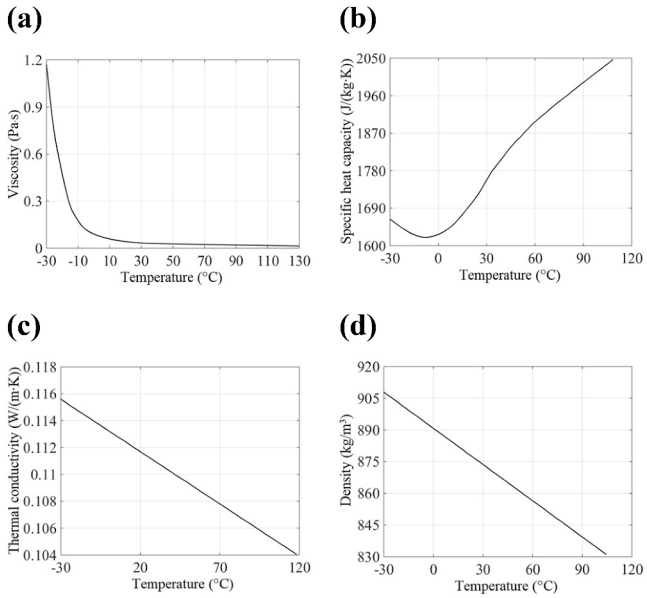

FIGURE 5 Transformer oil physical properties with temperature (a) Viscosity, (b) specific heat capacity, (c) thermal conductivity, and (d) density.

until convergence is reached, and the transformer winding temperature distribution is obtained. The coupled analysis flow chart of the fluid network model and the numerical analysis model with partition decoupling, that is, Scheme I is shown in Figure 6a.

Copper loss is the main heat source in the transformer. The resistivity of copper is a function of temperature as the independent variable as shown below.

$$P_{cu} = I^2R[1 + \alpha(T - T_0)] \quad (5)$$

where P_{cu} is the copper loss, I is the current, R is the is the resistance of the winding, α is the temperature coefficient and for copper, whose value is generally taken as 0.004/°C, and T and T_0 are the actual and initial temperatures of the windings, respectively. Therefore, the copper loss of the transformer varies with temperature.

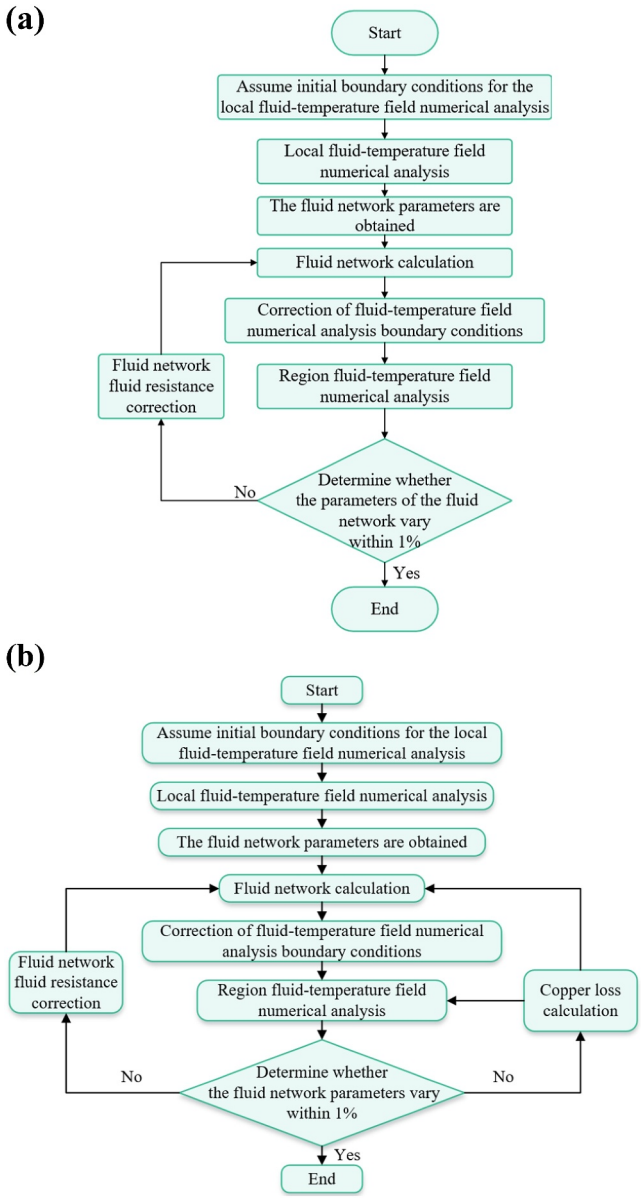

FIGURE 6 Flow chart. (a) Scheme I. (b) Scheme II.

To study the effect of copper loss variation with temperature on the temperature distribution results, the following three schemes are discussed in this paper. The Scheme I ignores the effect of temperature on copper loss, Scheme II is to correct the copper loss according to the winding average temperature based on Equation (5) and iterate the calculation, and the flow chart is shown in Figure 6b. Different from the calculation flow in Figure 6a, the flow in Figure 6b adds the process of copper loss correction. After obtaining the temperature distribution of the transformer, the copper loss is recalculated based on the obtained temperature distribution and the corrected copper loss is used again for the fluid-temperature characteristic solution. Scheme III is based on Scheme II by applying a temperature-dependent dynamic load to the 3D fluid-temperature field numerical analysis model, and

its fluid network calculation is consistent with the second scheme.

3 | RESULTS AND DISCUSSION

3.1 | Fluid network calculation results

The analysis was performed according to the flow chart design of Scheme I, and the obtained oil flow rate for each branch is shown in Figure 7.

The oil flow in the winding branch is mainly affected by the oil channel size and winding loss. The high, medium, and low voltage windings are arranged sequentially from outside to inside. The oil channel size decreases, and the flow resistance increases in turn. On the other hand, the winding losses provide thermal buoyancy for the oil flow. The high, medium, and low voltage winding losses decrease in order. The flow rate decreases with the increase in flow resistance and the decrease in winding loss. The loss loading methods of Schemes II and III are different, but the fluid network calculation results are the same. The winding losses of the three schemes are shown in Table 2.

The inlet velocity of each winding calculated by the fluid network is shown in Table 3, where the relative values are calculated using the value of Scheme I as the reference value.

Comparing the fluid network results for the three schemes reveals that there is also a degree of coupling between the change in winding losses and the flow rate. It is because in the winding branch of the fluid network model, when the oil flow rate is kept constant, the winding loss decreases, which causes the oil flow temperature to decrease as well. Then it leads to a subsequent increase in the gravitational pressure of the oil flow. To ensure pressure balance with the other parallel winding branches, the pressure that powers the oil flow then decreases, which in turn leads to a decrease in flow rate.

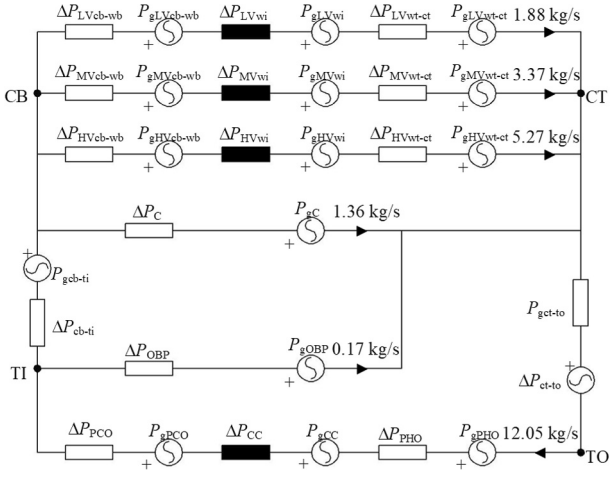

FIGURE 7 The oil flow rate for each branch according to scheme I.

TABLE 2 The loss value of windings.

Scheme number	High-voltage winding (W)	Medium-voltage winding (W)	Low-voltage winding (W)
Scheme I	264,957	153,363	47,587
Scheme II	265,891	152,264	47,165
Scheme III	265,878	152,170	47,147

3.2 | Fluid field results of the windings and radiator

The obtained fluid distribution inside the transformer for the three schemes is similar and has the same characteristics. Therefore, only the fluid field distribution of Scheme I is analysed.

The traces of oil flow in the radiator are shown in Figure 8. After the fluid network calculation, the inlet flow velocity is 75.63 mm/s. The transformer oil enters the radiator from the upper inlet of the radiator. After that, it enters each fin through the radiator duct and undergoes heat exchange. After dissipating the heat, the transformer oil converges at the lower radiator duct and then re-enters the transformer oil tank.

TABLE 3 Comparison of the inlet velocity of each winding.

Item	High-voltage winding (mm/s)	Medium-voltage winding (mm/s)	Low-voltage winding (mm/s)
Scheme I	47.96	42.78	34.15
Scheme II, III	48.01	42.60	33.98
Relative change (%)	+0.104	−0.421	−0.498%

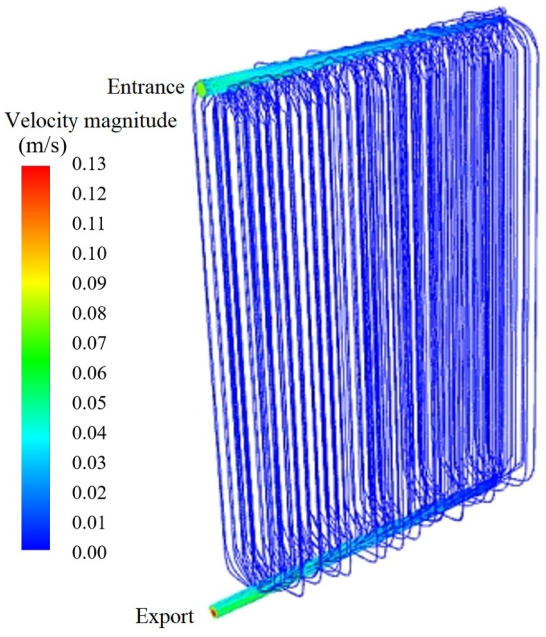

FIGURE 8 The traces of oil flow in the radiator.

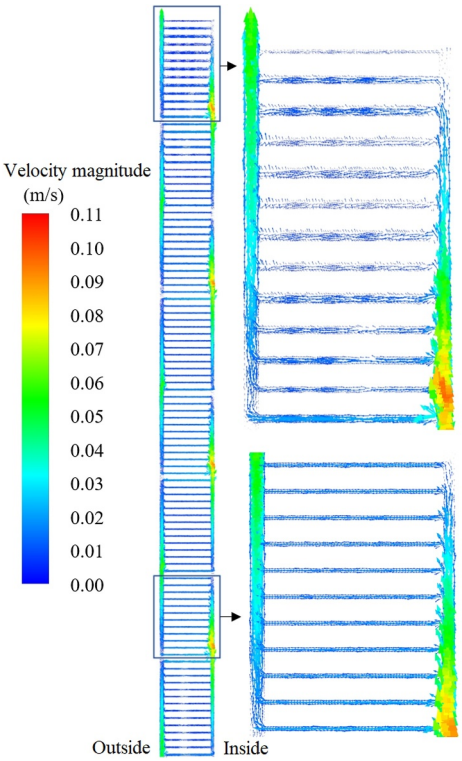

FIGURE 9 The flow velocity vector inside the high voltage winding.

The flow velocity vector diagram inside the high voltage winding is shown in Figure 9. As can be seen from the figure, the position with the highest flow velocity is at the confluence of the axial oil passage on the inner side of the high-voltage winding, with a maximum velocity of 106 mm/s. This is because the oil flowing through the winding will converge at the corresponding position of the oil baffle in the inner and outer axial oil passages. The cross-sectional area of the inner axial oil passage is smaller than that of the outer axial oil passage, so the highest flow velocity in the winding is located at the convergence of the inner axial oil passage.

It can also be seen from the figure that in the eight-segment structure of the high-voltage winding, the average flow velocity in the radial oil path of the second and third segments of the winding counting from the bottom to the top is 14.9 mm/s, and the average flow velocity in the radial oil path of the eighth segment winding is 9.8 mm/s, which is 34.2% lower than that of the second segment. The average flow velocity of oil between the uppermost winding of the eighth section winding and the insulating pad is 4.5 mm/s, which is 54.1% slower than the average radial flow velocity of this segment winding. It is due to the fact that the thickness of the oil channel pad used at the upper end of the transformer is greater than in other regions. For the same oil flow rate, the sectional area of the winding radial oil path is also larger in the region with the thicker oil channel pad, resulting in a lower oil flow velocity. On the other hand, within the same segment of winding, the thickness of the oil channel pad used between the uppermost winding and the insulation pad is smaller. It results in higher flow resistance and lower flow velocity.

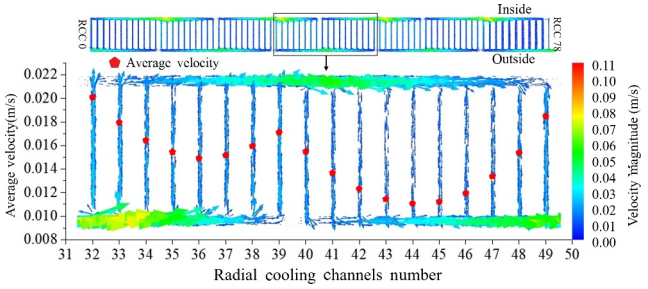

FIGURE 10 The flow velocity vector inside medium-voltage winding.

To study the radial oil flow distribution law in the 'oil baffle-winding-oil baffle', the fourth and fifth segments of the winding counting from the bottom to the top of the eight segments of the medium voltage winding structure were intercepted for analysis, that is, the 18 radial flow paths between the 32nd to 50th discs with the same height of the pad. Due to the position of the oil baffle plate, the number of radial flow paths in the two sections is unevenly distributed, in which 8 axial oil paths in the 32nd–40th discs belonging to the 4th segment winding and 10 oil paths in the 40th–50th discs belonging to the 5th segment winding.

The flow velocity vector diagram of the oil flow inside the medium voltage winding is shown in Figure 10. As can be seen from the figure, at the same flow rate, the lower the number of radial oil channels, the faster the oil flow velocity between the windings. The average flow velocities of oil flow within the radial oil channels of the fourth and fifth winding segments are 16.6 and 13.4 mm/s, respectively, and the former is 19.3% higher than the latter. Within the same segment of winding, the flow resistance of the oil path located in the middle position is higher, resulting in a smaller oil flow velocity. The lowest flow velocities in the middle of the two winding segments were 14.9 and 11.1 mm/s, which were 10.2% and 17.2% lower than the average flow velocities, respectively. In addition, since the cross-sectional area of the outer axial oil circuit is larger than that of the inner one, the flow resistance of the outer axial oil path is smaller and the flow rate is higher. The flow velocities in the oil paths of the two windings near the outer baffle are 20.1 and 18.5 mm/s, respectively, which are 14.9% and 16.2% larger than the flow velocities of 17.1 and 15.5 mm/s in the oil paths near the inner baffle. The oil flow distribution characteristic of low-voltage winding is the same as that of medium-voltage winding, so there is no special description.

3.3 | Temperature field results of the windings obtained in Scheme I

The temperature contours of the symmetrical sections of the high-voltage, medium-voltage and low-voltage windings obtained in Scheme I are shown in Figure 11.

As seen from the figure, the hot spot temperatures of the high-voltage, medium-voltage, and low-voltage windings are 89.43, 86.33, and 80.96°C, respectively. The temperature of the transformer oil is showing a tendency to step up as the axial

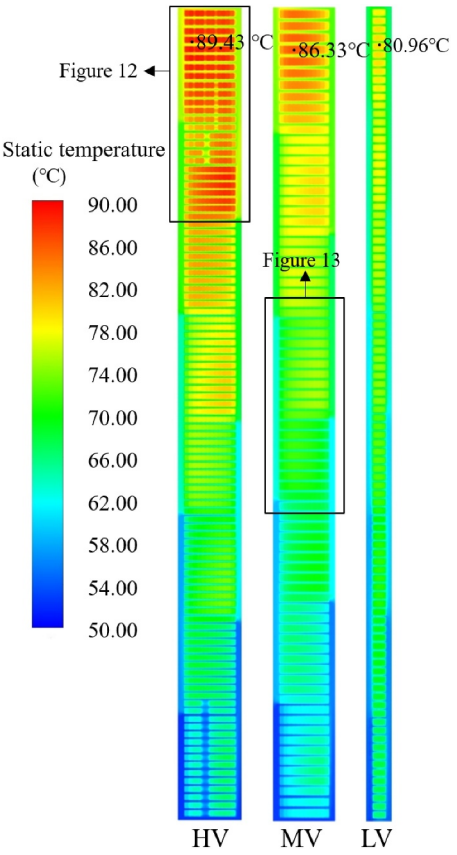

FIGURE 11 Temperature contour of the symmetrical sections of the windings obtained in Scheme I.

height increases. This is because the guiding effect of the oil baffle plate causes the axial oil channel to interrupt. There is an obvious temperature difference between the axial oil channel above and below the interrupt position. And it can also be found that the winding temperature also shows an increasing trend with the increase in axial height.

The temperature distribution contour of the 7th and 8th segments of the high voltage winding is shown in Figure 12. It can be seen that the hotspot temperature of the upper two windings is 18.5°C higher than that of the average oil temperature in the segment. The hotspot temperature of the other windings is only 17.4°C higher than that of the average oil temperature in the segment. It is because the upper part of the high-voltage winding uses a thicker oil channel pad, resulting in a slower oil flow in its radial oil path. Even though screen lines exist at the upper end of the winding and the heat source density is lower than in other locations. However, the increment of the hotspot temperature of the winding at the upper end over the average oil temperature in the segment is still higher than in the other locations. It indicates that the heat dissipation effect of using thinner oil channel pads for the windings between different oil channel pads is better. On the other hand, the arrangement of the screen line at the upper end of the high-voltage winding leads to the complexity of the temperature distribution at the upper end of the high-voltage winding.

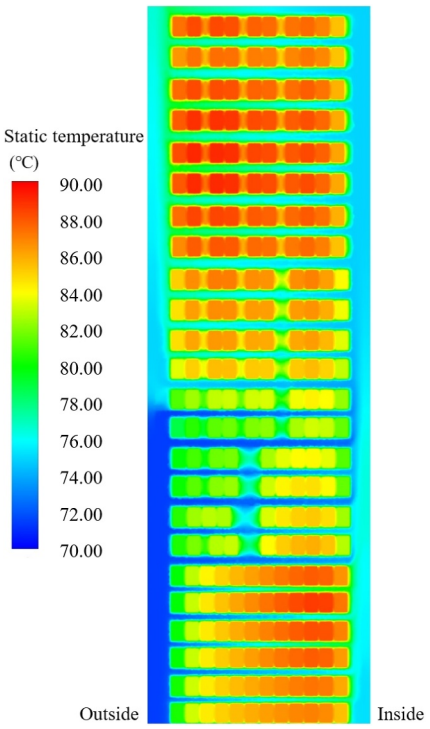

FIGURE 12 Temperature distribution contour of the 7th and 8th segments of the high voltage winding.

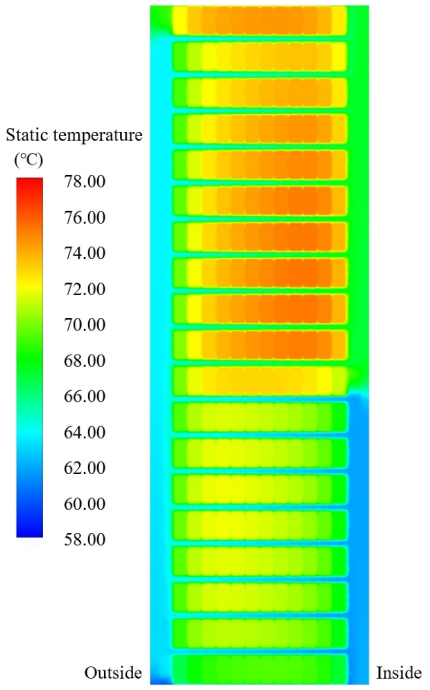

FIGURE 13 Temperature contour of the 32nd–50th discs of the medium voltage winding.

The temperature contour of the 32nd–50th discs of the medium voltage winding is shown in Figure 13. No. 32, No. 40, and No. 50 windings are located between the 3rd, 4th, 5th, and 6th segment windings of the medium voltage winding,

counting from bottom to top, and their temperatures are influenced by the temperature of oil flow between different segments on both sides. The hot spot temperatures are 67.76, 73.51, and 74.89°C, respectively.

For the fourth and fifth segment windings of the medium voltage winding, the hotspots in the segment are located in the No. 37 disc and No. 43 disc with temperatures of 73.34 and 76.78°C, respectively. The hotspot temperatures of the No. 33 and No. 49 discs near the inner oil baffle are 71.17 and 73.76°C, respectively. The hotspot temperatures of No. 39 and No. 41 discs near the outer oil baffle are 71.92 and 75.16°C, respectively. From the analysis of fluid results mentioned above, it is clear that the flow resistance of oil flow in the middle of the section 'oil baffle–winding–oil baffle' is the largest and the flow velocity is the smallest, so the heat dissipation is the worst. The radial oil path near the outer oil baffle has the lowest resistance and the largest flow velocity, so it has the best heat dissipation effect. Therefore, in a segment of winding, the heat dissipation effect of both sides is better than the middle. Therefore, the hotspot in the axial direction is located in the middle of the winding on the side close to the inner oil baffle. On the other hand, in the radial direction, the temperature of the oil flow in the radial oil channel gradually increases as the radial distance gradually increases. So, the hotspot radial position is located in the middle, towards the direction of oil flow. The temperature distribution of the low-voltage winding is similar to that of the medium-voltage winding, showing an overall step increase, with the local area high in the middle and low on both sides, which is not described in detail here.

3.4 | Comparison and analysis of the winding temperature of three schemes

The temperature distributions obtained from the three schemes have the same distribution characteristics, but there are some differences in the specific values. This is because the coupled calculation takes into account the effect of temperature variation on copper loss. In turn, the change in copper loss will cause a change in the oil flow rate. As the loss increases, the oil flow also increases together, which in turn will weaken the effect of the loss on the temperature distribution but will not change the nature of the coupling relationship. Therefore, in this paper, when analysing the effect of coupling calculation on the temperature distribution, only the loss aspect is explained, and the oil flow change is not mentioned.

The hotspot temperatures of the windings obtained for the three schemes are shown in Table 4, where the relative errors are all calculated based on the smaller side of the scheme number. The maximum temperatures of the wire discs of the high-voltage, medium-voltage, and low-voltage windings obtained for the three schemes are shown in Figure 14.

In the calculation process, the conductivity of copper at 75°C is used in Scheme I to calculate the winding copper loss. The average winding temperatures for the calculated copper loss of the high-voltage, medium-voltage, and low-voltage windings for Schemes II and III are 75.75, 72.01, and 71.59°C, respectively. Combining the data in the figures and tables, it can be seen that when the average temperature of the windings is higher than 75°C, the heat source density at each point of Scheme II is greater than that of Scheme I. Therefore, its temperature at all points is greater than that of Scheme I, and vice versa. For Schemes II and III, the top heat source density of Scheme III is greater than that of the top heat source density of Scheme I. The bottom heat source density of Scheme III is less than the bottom heat source density of Scheme II due to the winding temperature. So the bottom temperature of Scheme III is less than that of Scheme II, but as the height rises, the temperature distribution obtained by Scheme III will exceed that of Scheme II at a certain height. When the average temperature of the conductor is higher than 75°C, the hotspot temperature obtained by Scheme III is the highest, followed by Schemes II and I. When the average temperature of the conductor is slightly lower than 75°C, the calculation result of Scheme III is similar to that of Scheme II.

TABLE 4 The hotspot temperature of the three schemes.

Loss coupling mode	High-voltage winding	Medium-voltage winding	Low-voltage winding
Scheme I	89.43°C	86.33°C	80.96°C
Scheme II	89.47°C	86.16°C	80.74°C
Scheme III	89.90°C	86.55°C	81.06°C
Relative error between Scheme I and II	+0.04%	−0.20%	−0.27%
Relative error between Scheme I and III	+0.53%	+0.25%	+0.12%
Relative error between Scheme II and III	+0.48%	+0.45%	+0.40%

4 | EXPERIMENTAL VERIFICATION

An experimental platform is built in order to verify the rationality of the developed model and the effectiveness of the proposed method. Fibre-optic temperature measurement experiments were performed on the prototype. The experimental ambient temperature was 25.3°C. The fibre optic installation position is shown in Table 5. The experimental platform is shown in Figure 15.

During the test, the transformer is operated under rated operating conditions. When the rate of change of winding temperature is maintained at 1 K/h and reaches more than 3 h, it is considered to have reached the thermal steady state. Record the winding temperature data for 1 h after reaching the thermal steady state and calculate the average value of the recorded data as the experimental value of the transformer temperature under rated operating conditions. A comparison of the measured values and the calculated values is shown in Table 6.

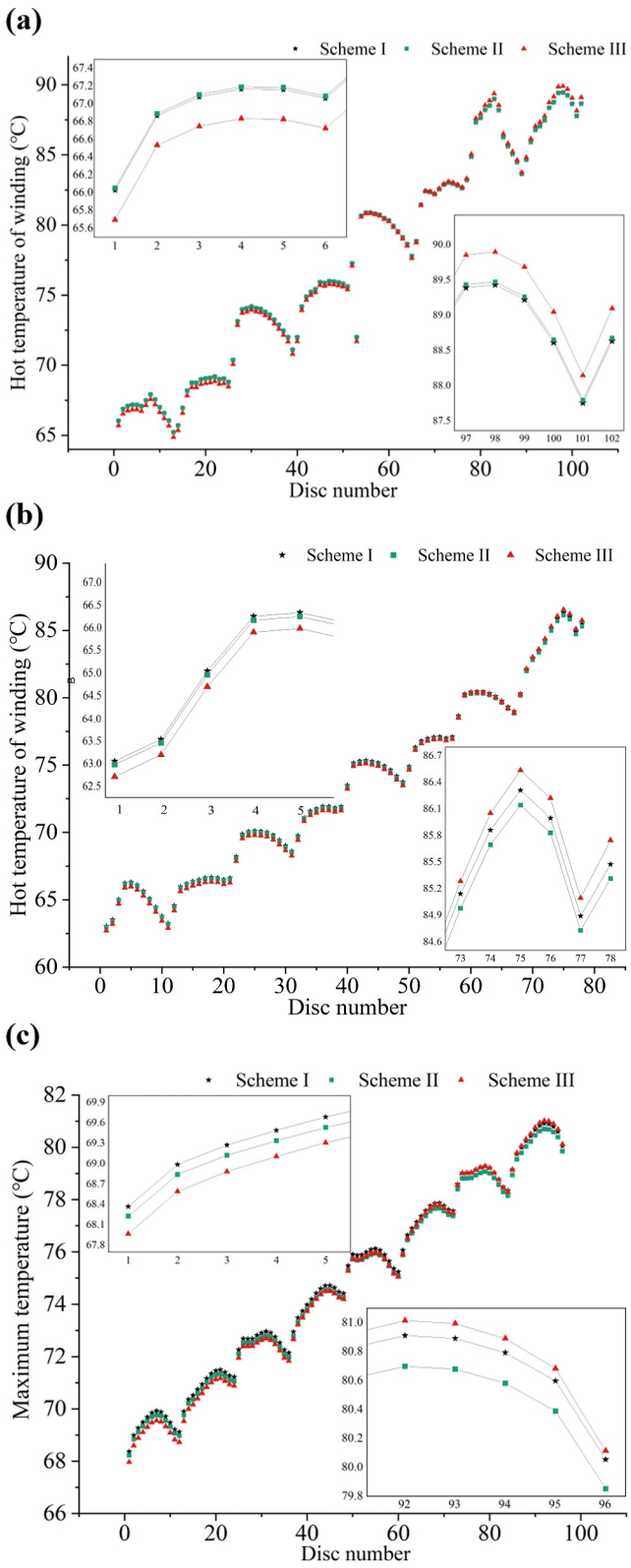

FIGURE 14 The maximum temperature of each wire disc. (a) High-voltage winding. (b) Medium-voltage winding. (c) Low-voltage winding.

The data in the table shows that the winding temperatures obtained based on fluid network decoupling satisfy engineering accuracy, and the calculation result of Scheme III has the highest accuracy. When the average temperature of the conductor is higher than 75°C, the accuracy of Scheme III is the highest, followed by Scheme II, and Scheme I is the lowest. When the average temperature of the conductor is lower than 75°C, the accuracy of Scheme III is close to that of Scheme I, and unidirectional coupling can be used for temperature solutions to save calculation time. However, the accuracy of Scheme II is lower at this time.

TABLE 5 The embedded position of optical fibre probe.

Item	Total number of wire discs	The probe position
High-voltage winding	102	96–98
Medium-voltage winding	78	74–76
Low-voltage winding	96	91–93

FIGURE 15 Experimental platform.

5 | CONCLUSION

This paper proposes a method for calculating transformer winding temperature based on fluid network decoupling. The following conclusions were obtained.

The local fluid-temperature field numerical analysis models of the windings and radiator were decoupled and solved based on the global domain fluid network. The temperature characteristics of the high voltage, medium voltage and low voltage windings were obtained and the hot spot temperatures of the three were 89.43, 86.33 and 80.96°C, respectively. The maximum relative error between the calculated values and measured values was 4.42%, which proved that the developed model and method are effective and accurate in studying power transformers with large capacities and complex ventilation structures.

TABLE 6 Measured values and calculated results.

Item		High-voltage winding	Medium-voltage winding	Low-voltage winding
Measured values (°C)		93.2	88.7	84.7
Scheme I	Hotspot temperature (°C)	89.43	86.33	80.96
	Relative error (%)	4.04	2.67	4.47
Scheme II	Hotspot temperature (°C)	89.47	86.16	80.70
	Relative error (%)	4.00	2.86	4.72
Scheme III	Hotspot temperature (°C)	89.90	86.55	81.02
	Relative error (%)	3.54	2.42	4.34

Due to the influence of oil flow distribution, the heat dissipation effect is better at the two ends than in the middle in a section of 'oil baffle–winding–oil baffle'. In multiple 'oil baffle–winding–oil baffle' sections, the heat dissipation effect of thick pads is weaker than that of thin pads.

Scheme III has the highest calculation accuracy. When the average temperature of the winding is slightly lower than 75°C, the results of Scheme I are closer to those of Scheme III, and Scheme I can be directly used for the solution to save calculation time. When the average temperature of the winding is higher than 75°C, the accuracy of Scheme III is the highest, followed by Scheme II, and Scheme I is the lowest.

ACKNOWLEDGEMENTS

This work was supported in part by the National Natural Science Foundation of China under Grants (52077047) and in part by the Natural Science Foundation of the Jiangsu Higher Education Institutions of China under Grants (22KJA470002).

CONFLICT OF INTEREST STATEMENT

The authors declare no potential conflict of interests.

DATA AVAILABILITY STATEMENT

Research data are not shared.

ORCID

Yongming Xu https://orcid.org/0000-0002-1122-0645
Ziyi Xu https://orcid.org/0000-0001-7861-5505
Yaodong Wang https://orcid.org/0000-0002-9697-8673

REFERENCES

1. Zhang, H., et al.: Improved information entropy weighted vague support vector machine method for transformer fault diagnosis. High Volt. 7(3), 510–522 (2022)
2. Darwish, M.M.F., et al.: A new technique for fault diagnosis in transformer insulating oil based on infrared spectroscopy measurements. High Volt. 9(2), 319–335 (2024)
3. Yang, L., et al.: Analysis of multi-objective optimisation method for main insulation structure configuration scheme of valve-side winding of ultra-high voltage converter transformer considering multi-field coupling. High Volt. 9(2), 296–308 (2024)
4. Gao, S., Yang, L., Ke, T.: Ageing characteristics and lifetime model of oil-paper insulation for oil-immersed paper condenser bushing. High Volt. 6(2), 278–290 (2020)
5. Radakovic, Z., et al.: Ratings of oil power transformer in different cooling modes. IEEE Trans. Power Del. 27(2), 618–625 (2012)
6. Radakovic, Z., Sorgic, M.: Basics of detailed thermal-hydraulic model for thermal design of oil power transformers. IEEE Trans. Power Del. 25(2), 790–802 (2010)
7. Radakovic, Z., Radoman, U., Kostic, P.: Decomposition of the hot-spot factor. IEEE Trans. Power Del. 30(1), 403–411 (2015)
8. Radakovic, Z., Jevtic, M., Das, B.: Dynamic thermal model of kiosk oil immersed transformers based on the thermal buoyancy driven air flow. Int. J. Electr. Power Energy Syst. 92, 14–24 (2017)
9. Cotas, C., et al.: Numerical study of transient flow dynamics in a core-type transformer windings. Elec. Power Syst. Res. 187, 106423 (2020)
10. Zhou, L., et al.: Transient thermal network model for train-induced wind cooling dry-type on-board traction transformer in electric multiple units. High Volt. 8(3), 514–526 (2023)
11. Taheri, A.A., Abdali, A., Rabiee, A.: Indoor distribution transformers oil temperature prediction using new electro-thermal resistance model and normal cyclic overloading strategy: an experimental case study. IET Generation, Transm. & Distrib. 14(24), 5792–5803 (2020)
12. Shiravand, V., et al.: Prediction of transformer fault in cooling system using combining advanced thermal model and thermography. IET Generation, Transm. & Distrib. 15(13), 1972–1983 (2021)
13. Shiravand, V., et al.: Improving the transformer thermal modeling by considering additional thermal points. Int. J. Electr. Power Energy Syst. 128, 106748 (2021)
14. Taheri, A.A., Abdali, A., Rabiee, A.: A novel model for thermal behavior prediction of oil-immersed distribution transformers with consideration of solar radiation. IEEE Trans. Power Del. 34(4), 1634–1646 (2019)
15. Wei, B., et al.: Three dimensional simulation technology research of split type cooling transformer based on finite volume method. Energy Proc. 141, 405–410 (2017)
16. Silva, J.R., Bastos, J.P.A.: Analysis of power transformer geometry simplifications on electromagnetic and thermodynamic simulations. IEEE Trans. Magn. 51(3), 1–4 (2015)
17. Mechkov, E., et al.: Thermal analysis using 3D FEM model of oil-immersed distribution transformer. In: 2016 19th International Symposium on Electrical Apparatus and Technologies (SIELA), Bourgas (2016)
18. Pontes, C.E.V., et al.: Thermodynamic models and three-dimensional analysis for determination of load limits transformers. IEEE Lat. Am. Trans. 11(5), 1225–1231 (2013)
19. Córdoba, P.A., Dari, E., Silin, N.: A 3D numerical model of an ONAN distribution transformer. Appl. Therm. Eng. 148, 897–906 (2019)
20. Stebel, M., et al.: Thermal analysis of 8.5 MVA disk-type power transformer cooled by biodegradable ester oil working in ONAN mode by using advanced EMAG–CFD–CFD coupling. Int. J. Electr. Power Energy Syst. 136, 107737 (2022)
21. Liu, C., et al.: Temperature rise of a dry-type transformer with quasi-3d coupled-field method. IET Electr. Power Appl. 10(7), 598–603 (2013)
22. Chi, C., et al.: A multi-scale thermal-fluid coupling model for ONAN transformer considering entire circulating oil systems. Int. J. Electr. Power Energy Syst. 135, 1–11 (2022)

23. Raeisian, L., et al.: Thermal management of a distribution transformer: an optimization study of the cooling system using CFD and response surface methodology. Int. J. Electr. Power Energy Syst. 104, 443–455 (2019)
24. Dasara, S., Mishra, V.: Shielding measures of power transformer to mitigate stray loss and hot spot through coupled 3D FEA. High Volt. 2(4), 267–273 (2017)
25. Santisteban, A., et al.: Thermal analysis of natural esters in a low-voltage disc-type winding of a power transformer. In: 2017 IEEE 19th International Conference on Dielectric Liquids (ICDL) (2017)
26. Wu, W., et al.: Computational fluid dynamics calibration for network modelling of transformer cooling flows – part II: pressure loss at junction nodes. IET Electr. Power Appl. 6(1), 28–34 (2012)
27. Santisteban, A., et al.: Thermal modelling of a power transformer disc type winding immersed in mineral and ester-based oils using network models and CFD. IEEE Access 7, 174651–174661 (2019)

How to cite this article: Xu, Y., et al.: Research on temperature distribution characteristics of oil-immersed power transformers based on fluid network decoupling. High Voltage. 9(5), 1136–1148 (2024). https://doi.org/10.1049/hve2.12488